



Plate 1 Satellite image of the Venice Lagoon.

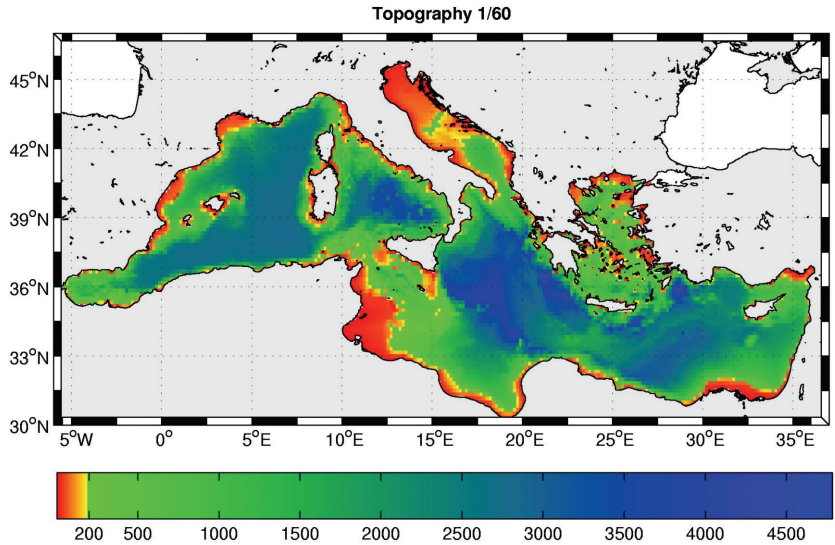
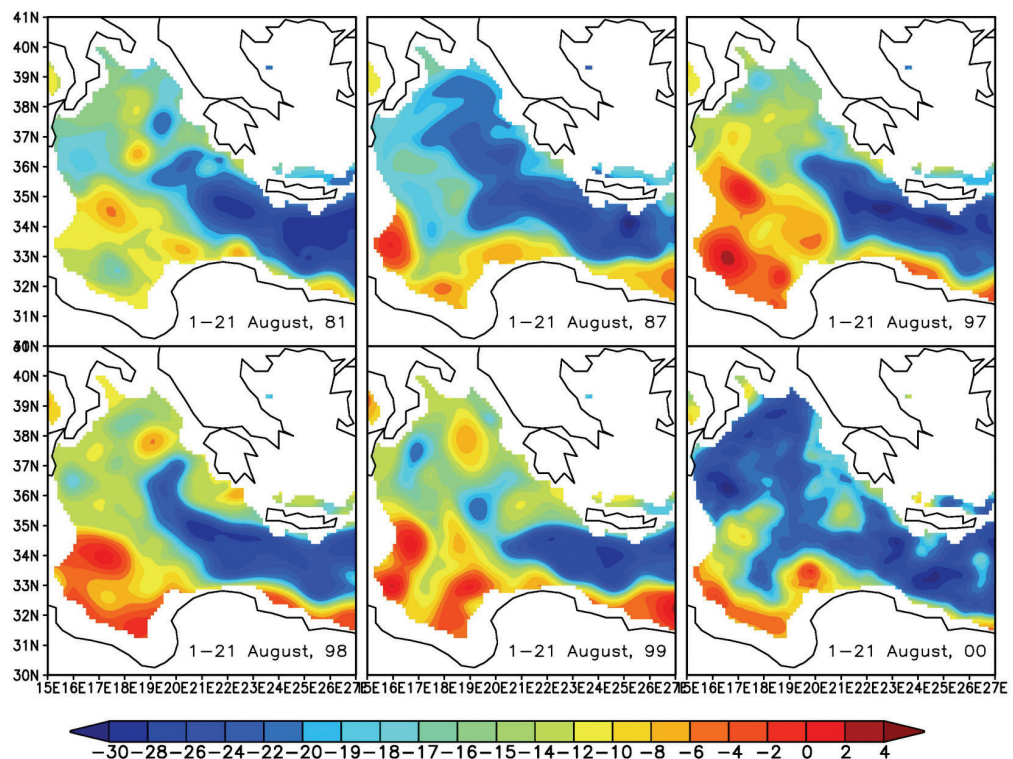


Plate 2 Bathymetry
(water depths in metres) of the Mediterranean Basin
(see Pinardi *et al.*, chapter 6).

Plate 3 Dynamic height anomaly at 5 m (with respect to 800 m reference level) in the eastern Mediterranean Sea for the month of August in selected years between 1981 (top left) and 2000 (bottom right). Units are in cm
(see Pinardi *et al.*, chapter 6).



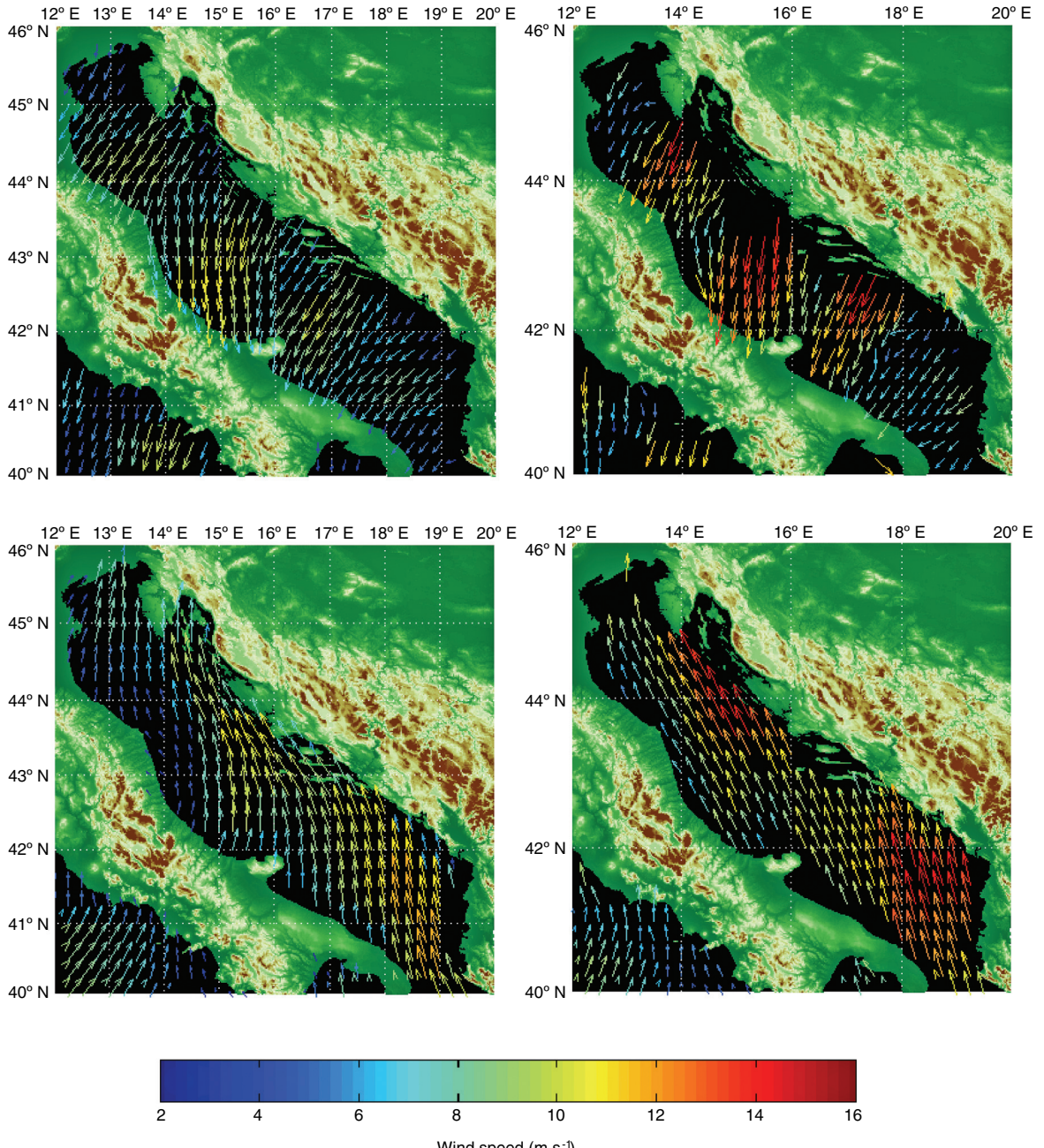


Plate 4 Adriatic Sea winds as described by satellite scatterometry (QuikSCAT) and modelled wind fields (ECMWF analysis). Top panels: *bora* wind (11 February 2001). Bottom panels: *sirocco* wind (25 January 2001). Left panels: wind field from the ECMWF analysis, interpolated over a 25 km by 25 km grid, respectively at 06:00 and 18:00 GMT. Right panels: QuikSCAT satellite scatterometer wind field at 04:08 and 16:56 GMT (see Zecchetto *et al.*, chapter 7).

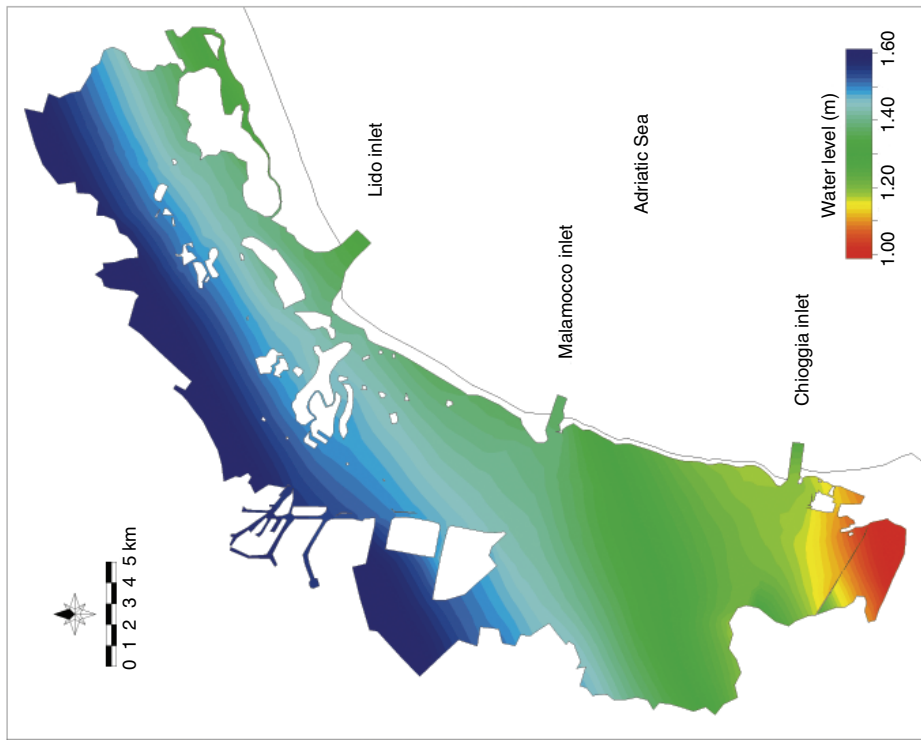


Plate 6. Spatial variability in maximum water level on 6 November 2000, showing the effect of a *sirocco* (SE) wind (see Ferla, chapter 12).

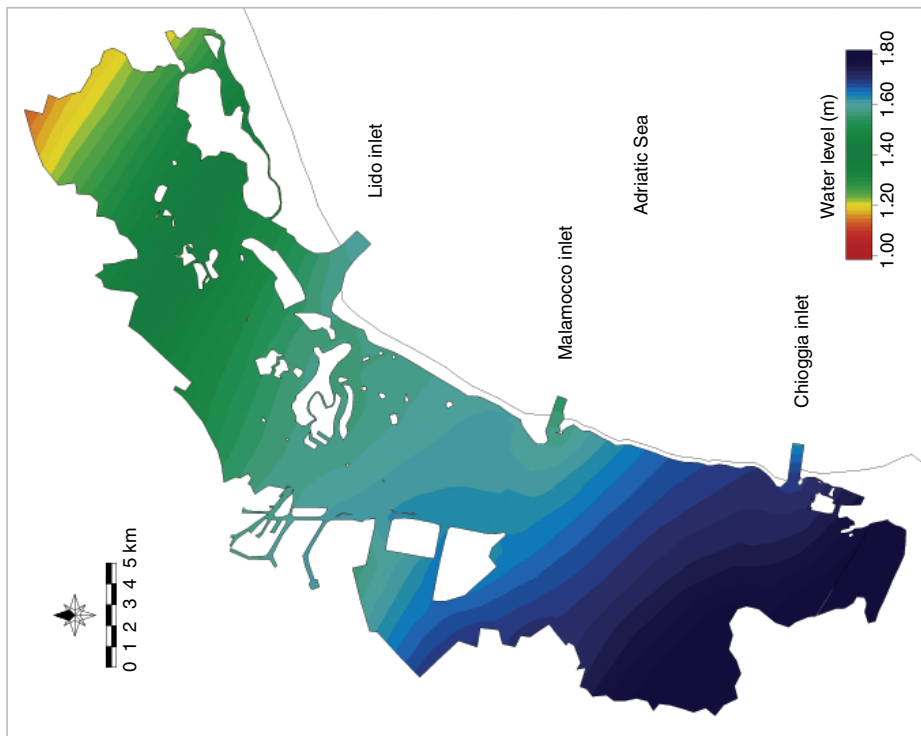


Plate 5. Spatial variability in maximum water level on 8 December 1992, showing the effect of a *bora* (NE) wind (see Ferla, chapter 12).

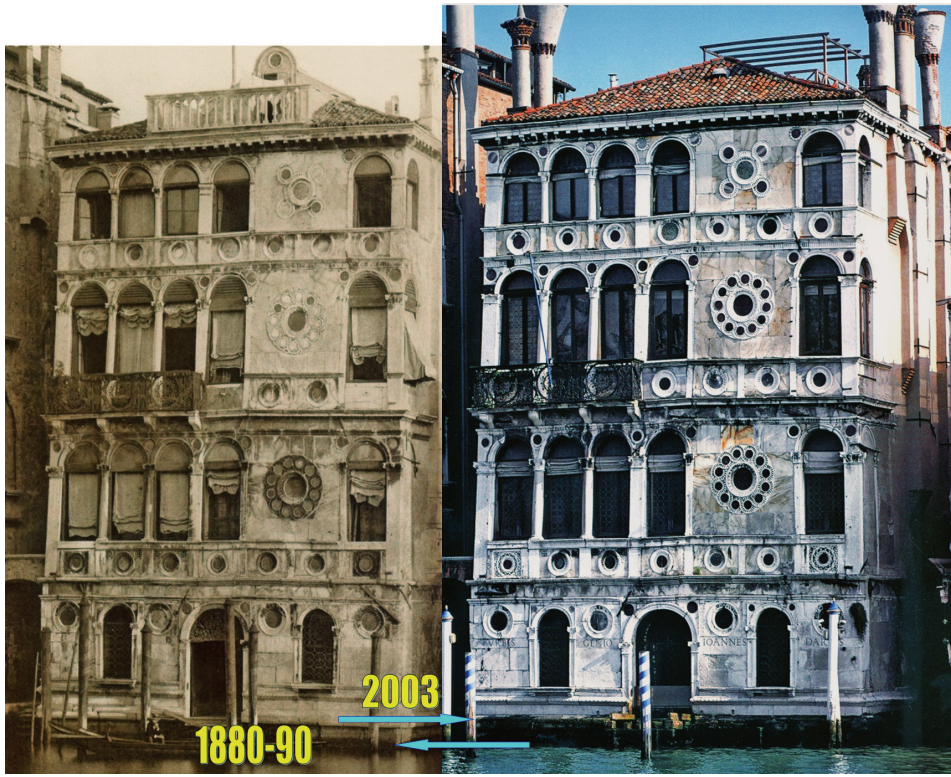


Plate 7 An early photograph (1880–90) of the Dario Palace in Venice (left) and a present day view of the same building (right). The observed algal displacement is 46 ± 10 cm (for the apparent sea-level rise subtract 13 cm with reference to the 2003 algal level) (see Camuffo *et al.*, chapter 16).

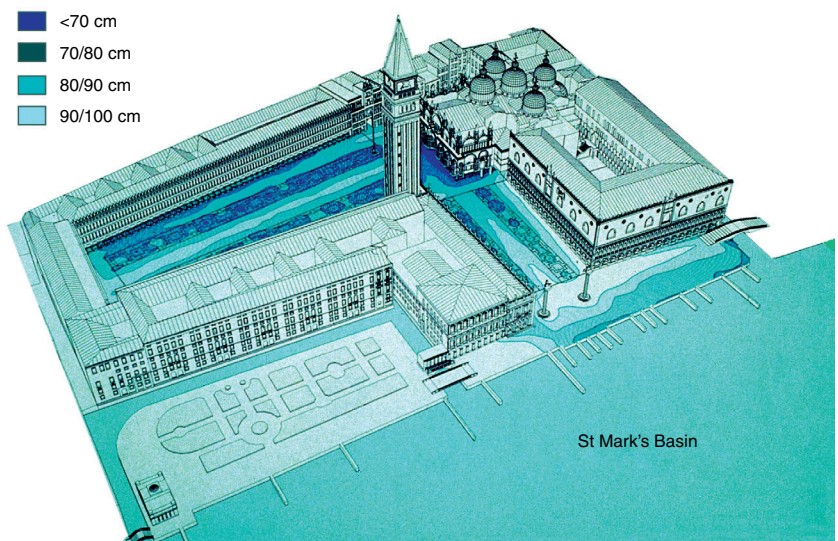


Plate 8 Flooding of St Mark's Square. Water levels relate to the 1897 reference level (present mean sea level lies at c. 25 cm above this level) (see Vio, chapter 21, and Brotto, chapter 23).



Plate 9 Fragment of a figurative fresco and detail in Venice (see Danzi *et al.*, chapter 24).

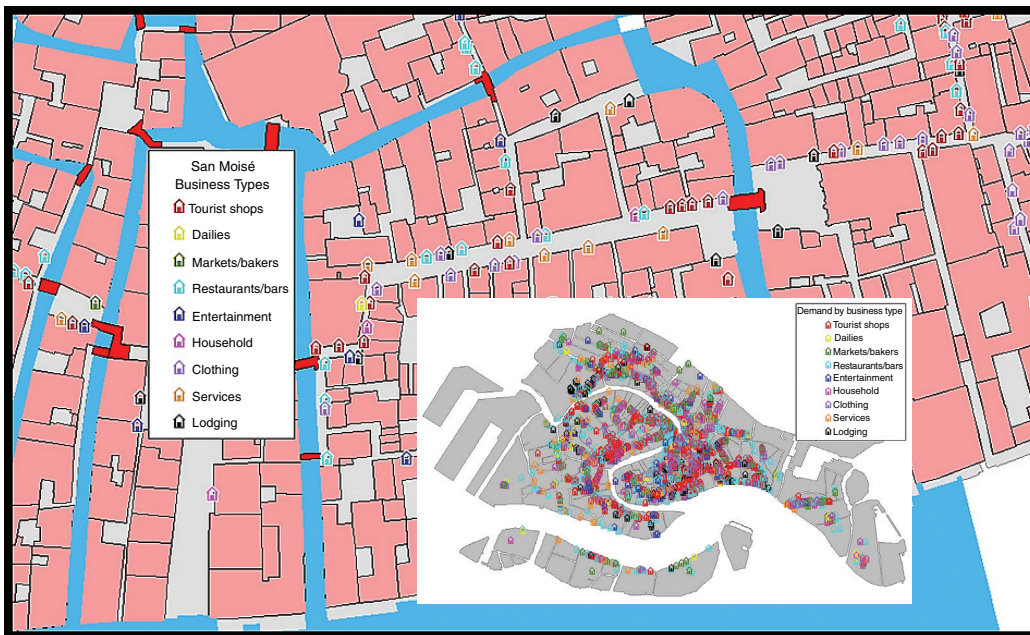


Plate 10 Inventory of all commercial establishments
in Venice by category (with detail for San Moisé)
(see Carrera, chapter 27).

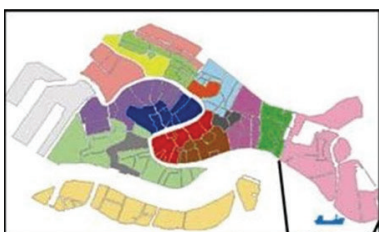
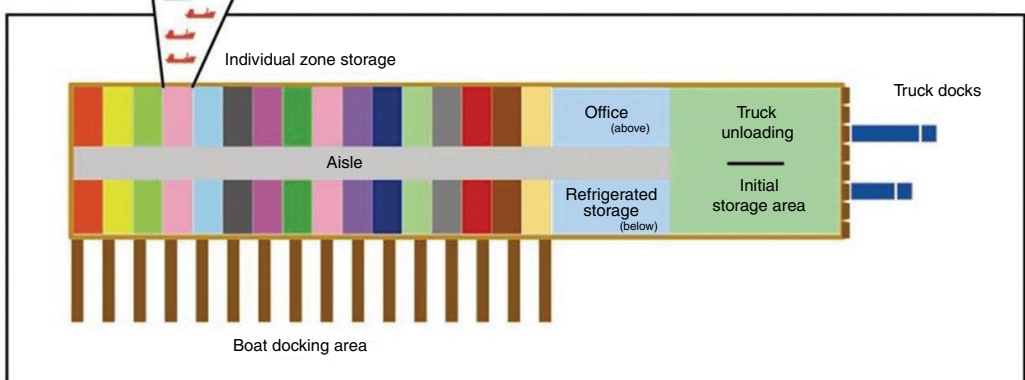


Plate 11 Proposed cargo warehouse at Tronchetto
with 16 bays, one for each of the delivery zones of the city
(see Carrera, chapter 27).



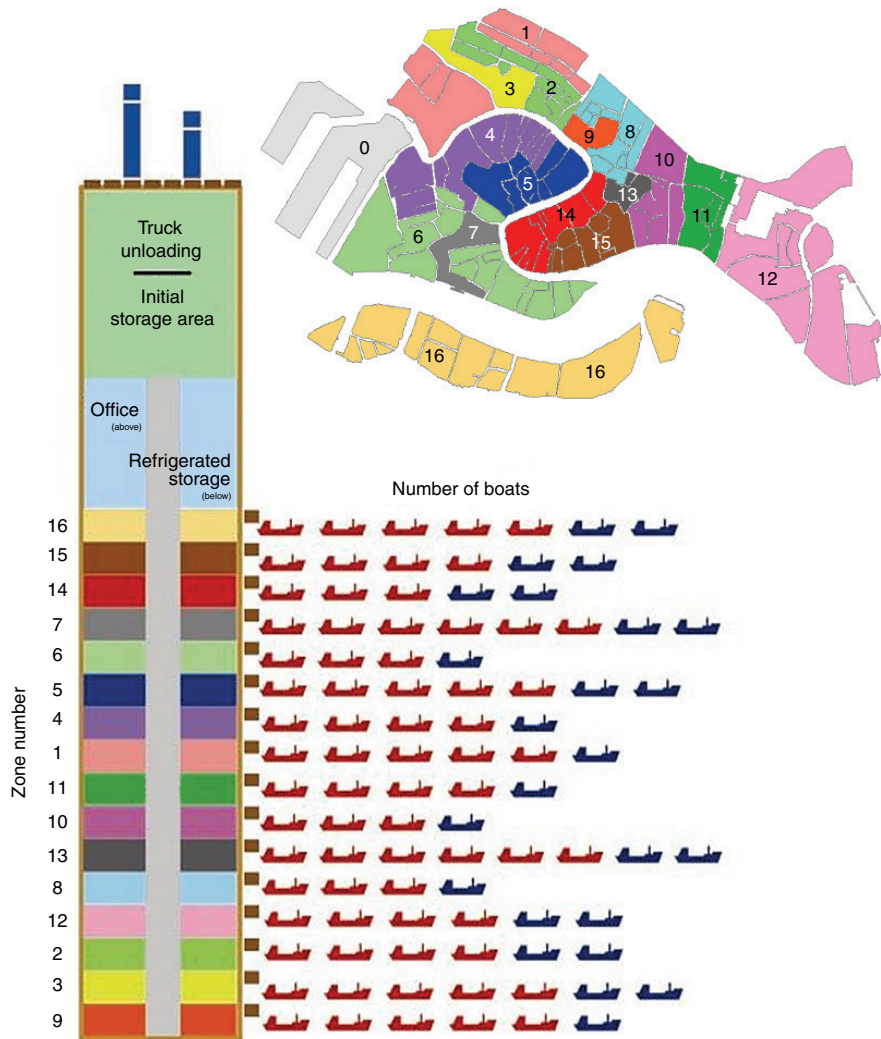


Plate 12 Proposed fleets of boats carrying dry (red) and refrigerated goods (blue) required to service each of the 16 homogeneous delivery zones (see Carrera, chapter 27).

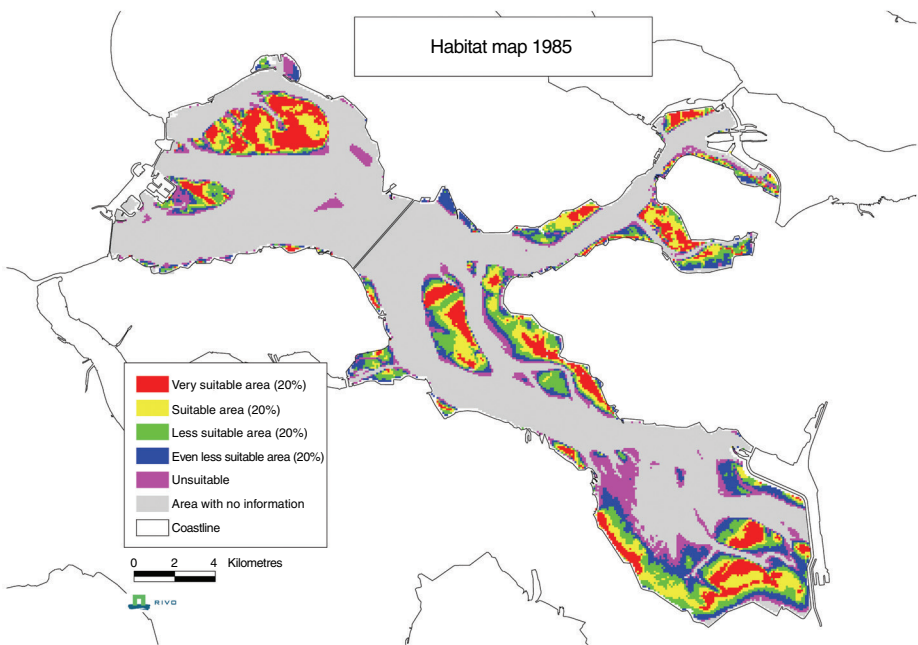


Plate 13 Cockle (*Cerastoderma edule*) habitat in the Oosterschelde, The Netherlands, in 1985 (source: RIVO-CSO (see Saeijs and Guerts van Kessel, chapter 30)).

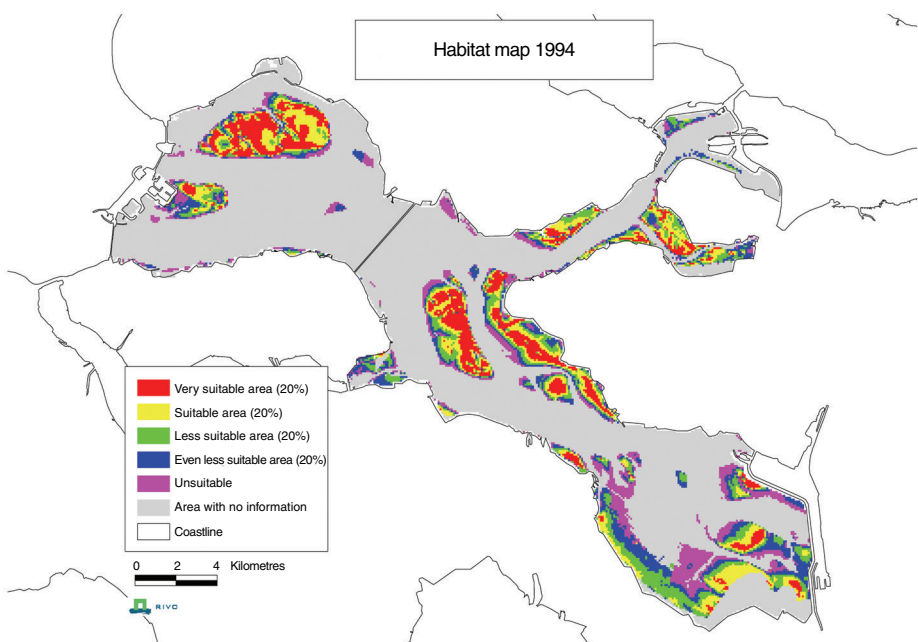


Plate 14 Cockle (*Cerastoderma edule*) habitat in the Oosterschelde, The Netherlands, in 1994 (source: RIVO-CSO (see Saeijs and Guerts van Kessel, chapter 30)).



Plate 15 Pacific oyster (*Crassostrea gigas*) reef in the Oosterschelde, The Netherlands (photograph: Dr N. Steins) (see Saeijs and Guerts van Kessel, chapter 30).

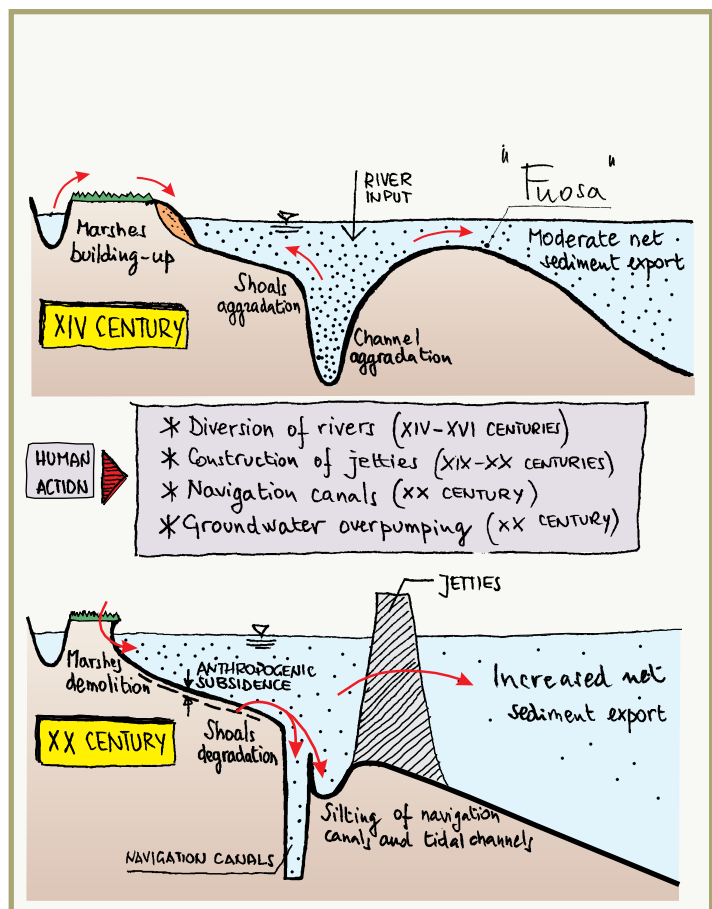


Plate 16 Lagoon conditions in the fourteenth (top) and twentieth (bottom) centuries (see Di Silvio, chapter 43).

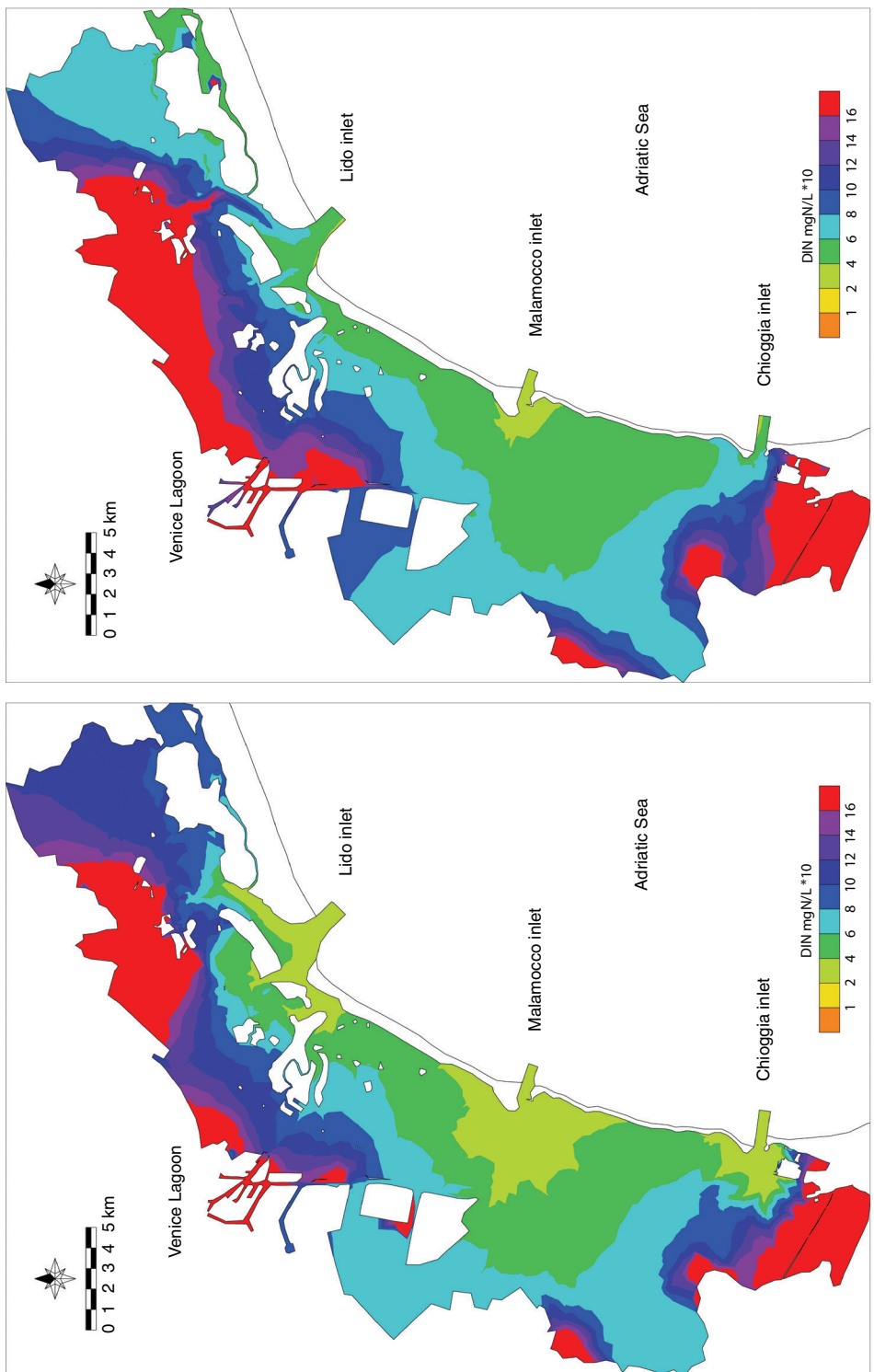


Plate 17 Spatial distribution of yearly averaged values of dissolved organic nitrogen (DIN) in the Venice Lagoon under climatological conditions (left) and realistic forcings (right) (see Umgieser *et al.*, chapter 47).

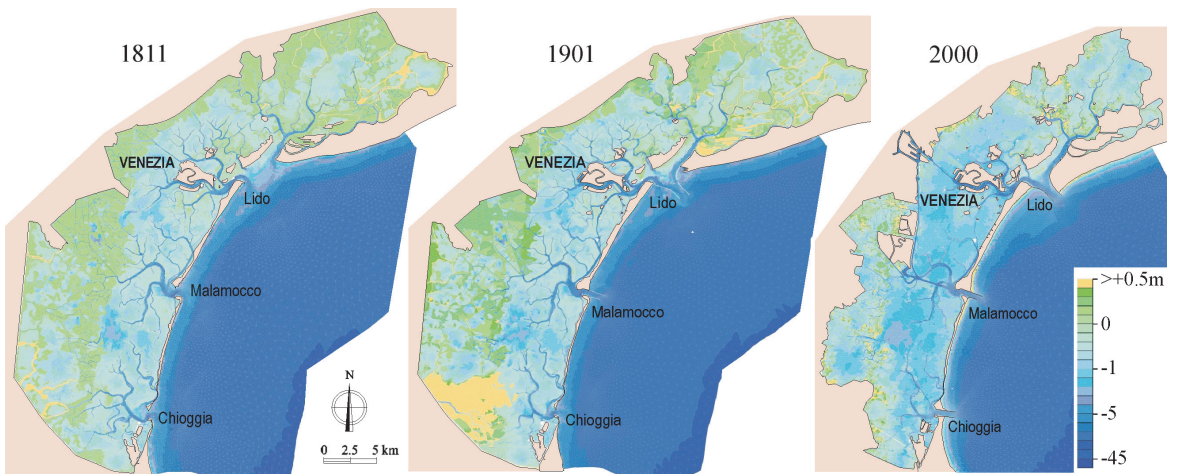
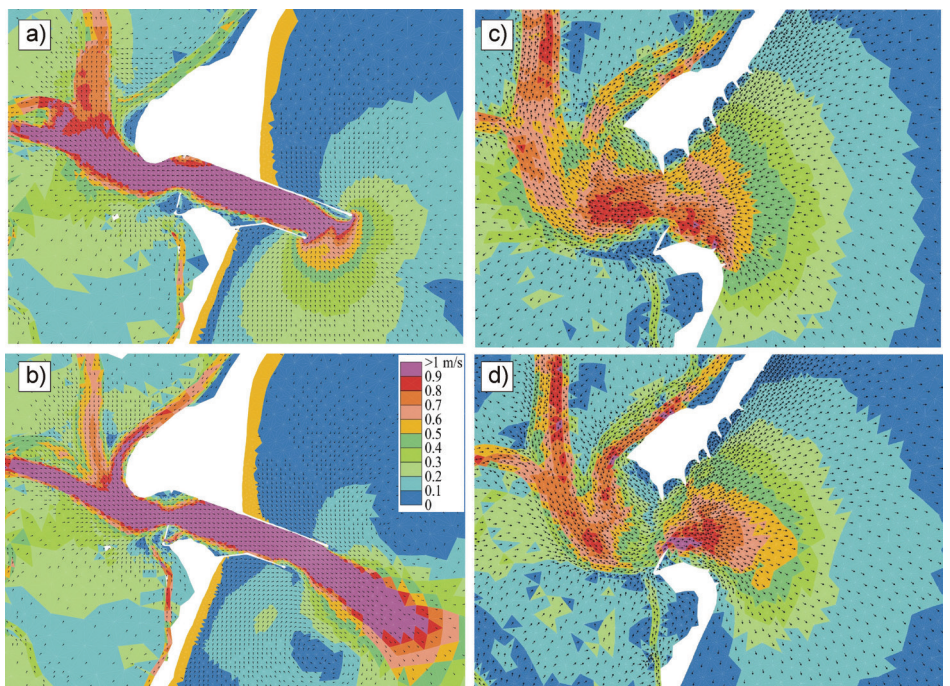


Plate 18 Bathymetric configurations of the Venice Lagoon surveyed in: (a) 1811; (b) 1901; and (c) 2000 (present configuration) (see D'Alpaos and Martini, chapter 48).

Plate 19 Examples of the velocity field at the Malamocco inlet to the Venice Lagoon. Flood phase (a, c) and ebb phase (b, d) in the present configuration (left) and for the 1811 configuration (right) (see D'Alpaos and Martini, chapter 48).



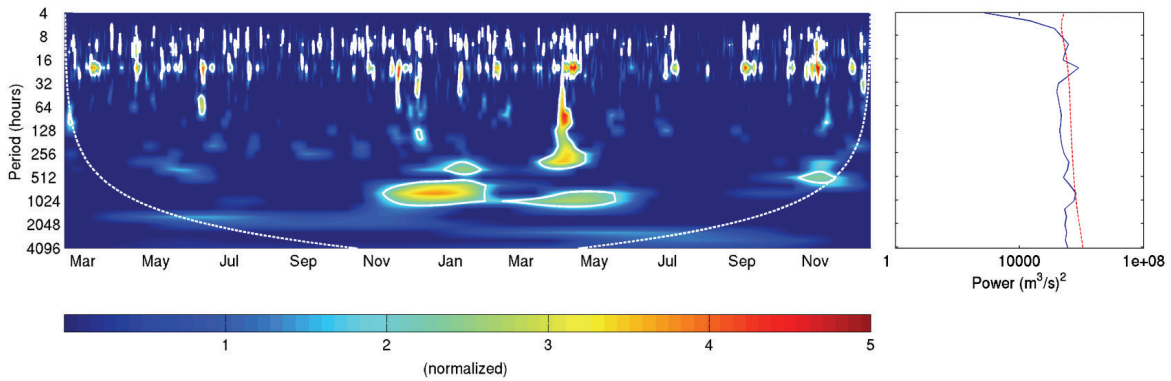


Plate 20 Wavelet spectrum of non-tidal water flux for Chioggia inlet (left panel). Wavelet spectrum values are normalized by the total variance, region under dashed line is affected by edge effects. On the right panel time-averaged wavelet spectrum is shown; dashed red line represents the background-noise spectrum with an autocorrelation of 0.14 for the lag 1 estimated from data (see Gačić, chapter 49).

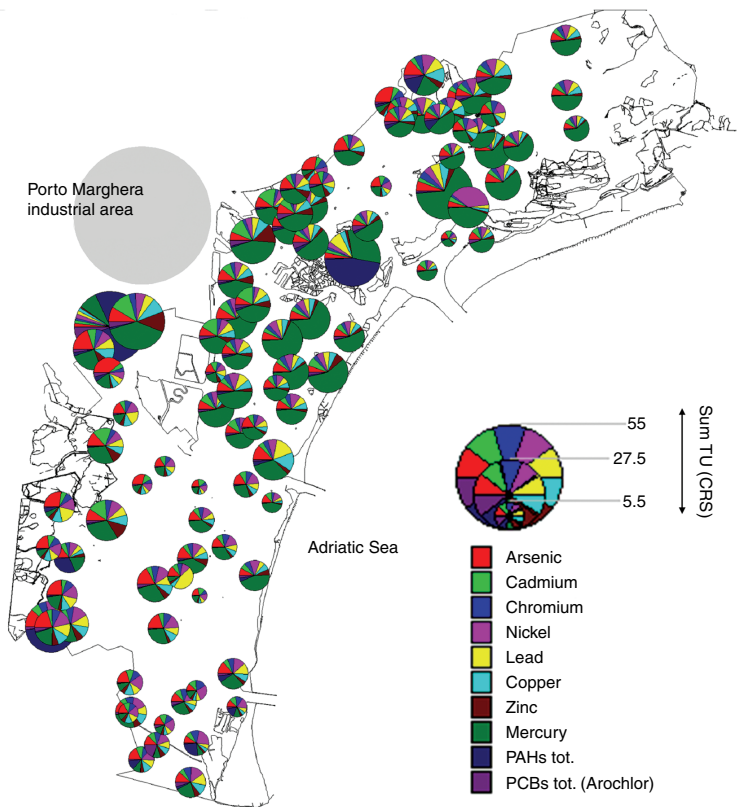


Plate 21 Pie chart visualization of the individual contaminant contribution to the cumulative risk (CRS) for the benthic community at sampling stations in the Venice Lagoon. The risk was estimated through the Toxic Units (TU) method and the ecotoxicological TEL benchmark (see Marcomini *et al.*, chapter 54).

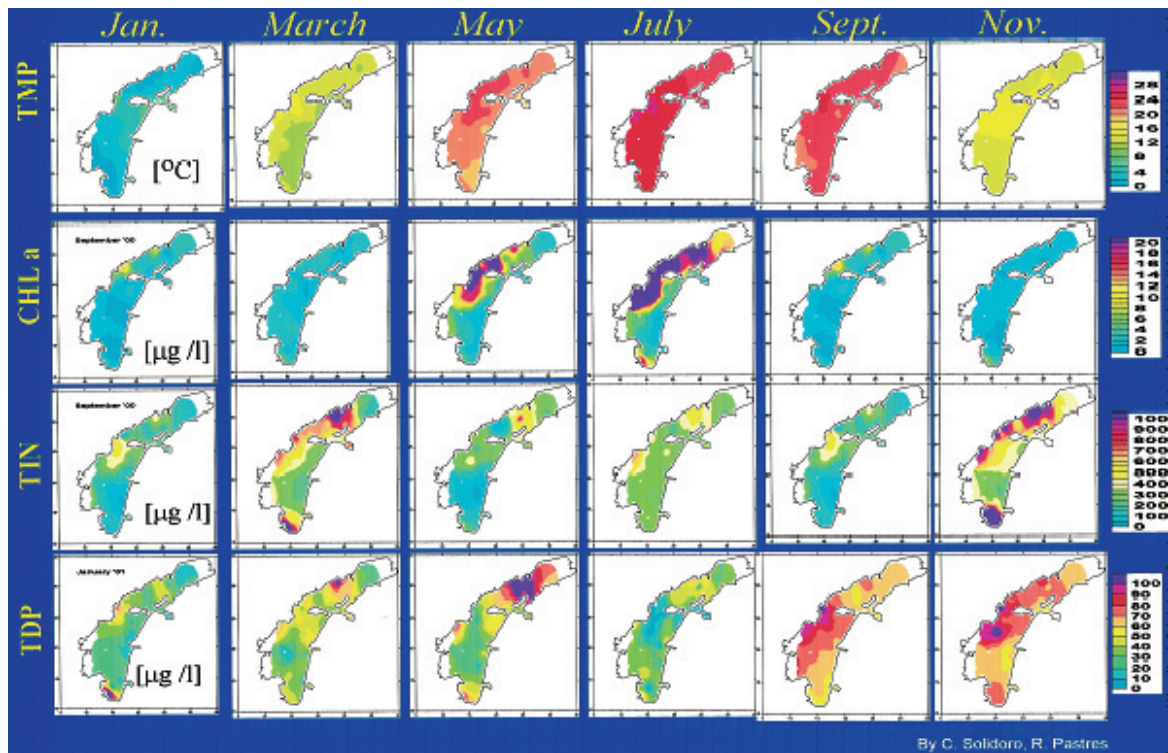


Plate 22 Temporal evolution of temperature (T), chlorophyll-a (CHL-a), total inorganic nitrogen (TIN) and total dissolved phosphorous (TDP) for the year 2001 in the Venice Lagoon (see Zirino, chapter 55).

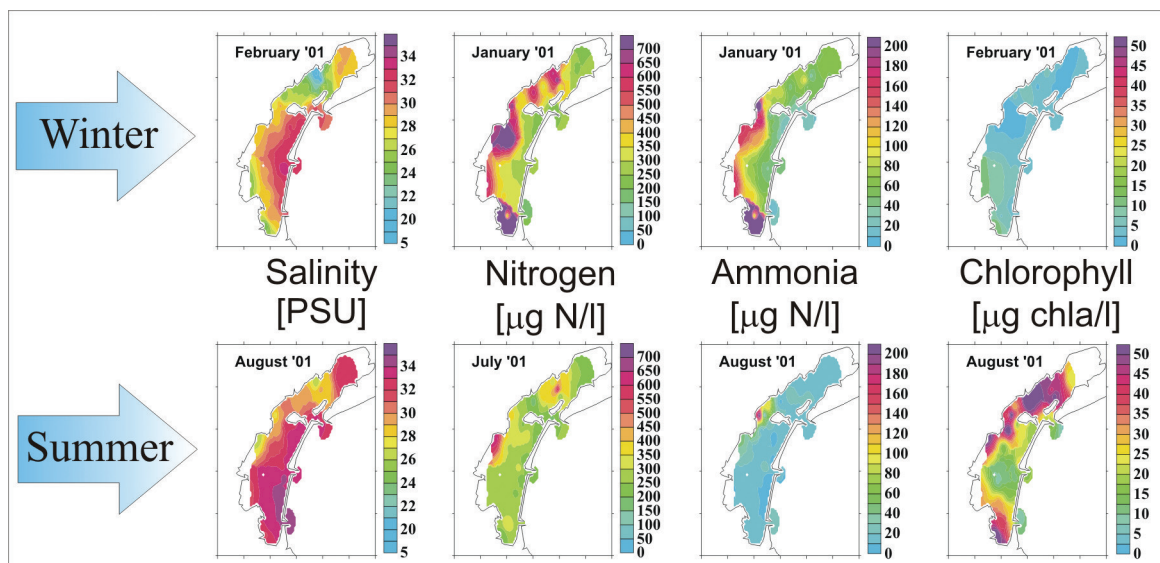


Plate 23 Typical salinity, nitrogen, ammonia and chlorophyll levels during winter and summer in the Venice Lagoon (see Penna *et al.*, chapter 56).

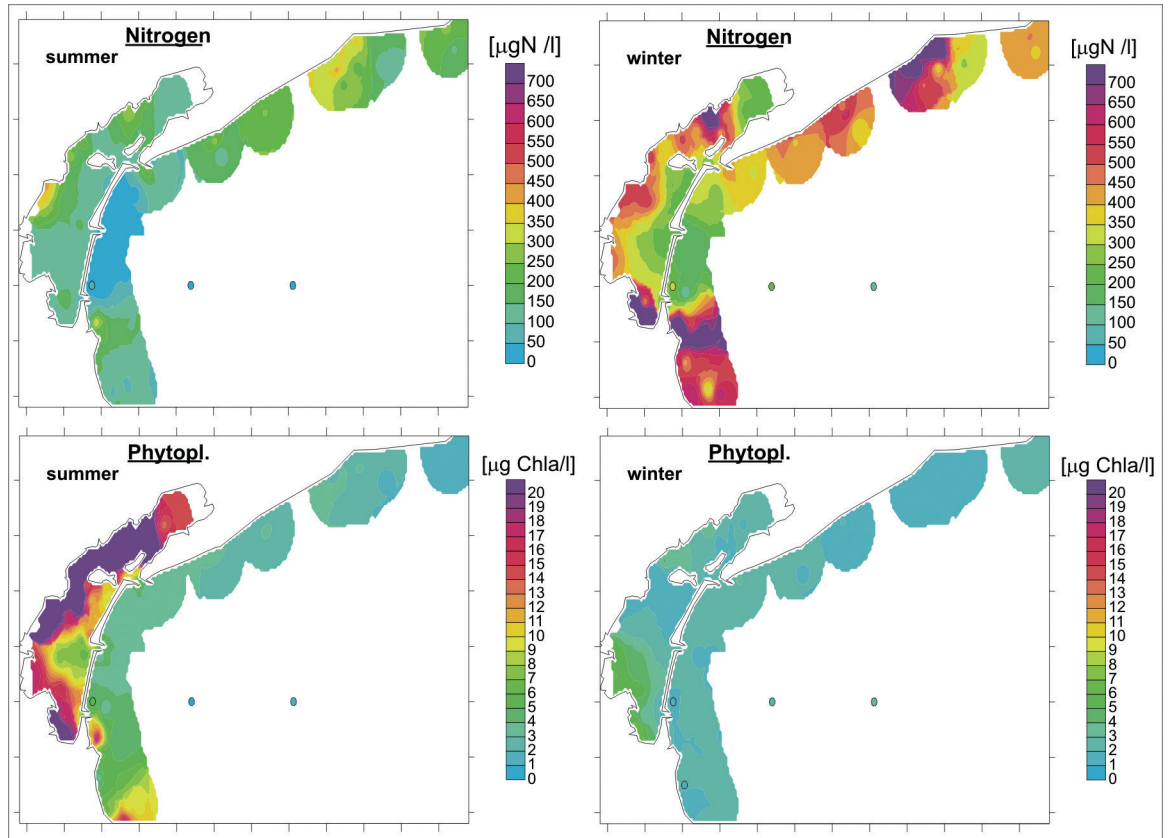


Plate 24 Examples of integrated data processing of water quality of the lagoon (Venice Water Authority and CVN) and the coastal area (ARPAV) in 2001 (see Penna *et al.*, chapter 56).

Plate 25 Distribution of (a) Zn and (b) Cu concentration in the upper sediment layer of the canal network. Colours indicate the relative magnitude of contaminant concentrations measured (mg/kg, dry weight) (see Zonta *et al.*, chapter 64, for explanation of white arrow).

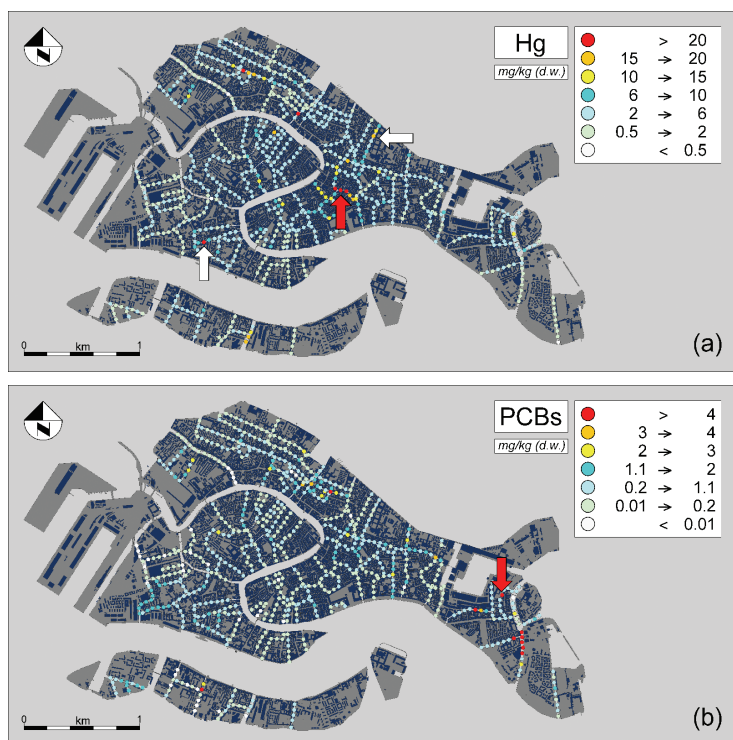
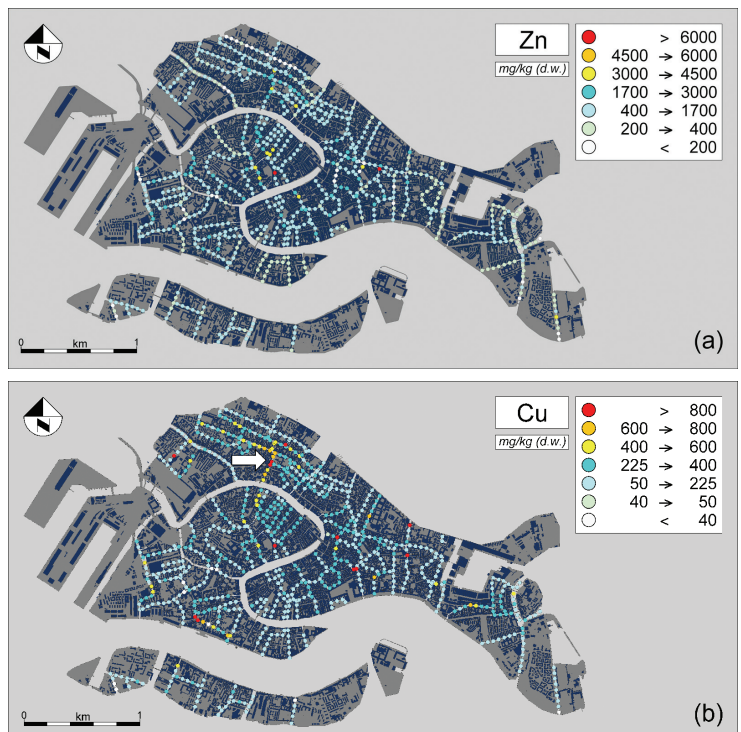


Plate 26 Distribution of (a) Hg and (b) PCBs concentration in the upper sediment layer of the canal network. Colours indicate the relative magnitude of contaminant concentrations measured (mg/kg, dry weight) (see Zonta *et al.*, chapter 64, for explanation of red and white arrows).